Field-directed Self-assembly of Multifunctional Magnetic-Plasmonic Core-shell Nanoparticles with Applications to Photonics

Xiaozheng Xue[1], Kai Liu[2], Jianchao Wang[1] and Edward P. Furlani[1,2]

[1]Dept. of Chemical and Biological Engineering, [2]Dept. of Electrical Engineering
University at Buffalo SUNY, Buffalo NY
Email: xiaozhen@buffalo.edu

ABSTRACT

Interest in the manipulation and self-assembly of magnetic nanoparticles has grown in recent years due to advances in particle synthesis and functionalization, which have led to a proliferation of applications that include the biomolecular transport, drug targeting, gene transfection, bioseparation, microfluidic mixers and bio and chemical sensors, among others. However, despite the growing application of magnetic nanoparticles, many fundamental aspects of their collective behavior remain unknown. In this presentation, we use computational modeling to demonstrate the self-assembly of magnetic core-shell particles into chain structures and the control of this process by carefully choosing particle properties and an applied field. Our analysis takes into account several competitive effects, including the induced magnetic dipole-dipole interactions, the electrostatic repulsion between particles based on DLVO theory, Brownian dynamics, Van der Waals interaction and a steric repulsive force caused by surfactant-surfactant contact. The model is used to study the self-assembly (chaining) of magnetic-plasmonic Fe_3O_4@Au core-shell nanoparticles that are confined to a nanochannel. Computational photonic analysis is used to compute the optical behavior of 1D multiparticle chains. Moreover, an analysis is performed to study the local profiles of thermal loss and electric field enhancement between adjacent nanoparticles. The ability to self-assemble the particles with tunable field enhancement holds potential for fundamental studies of light-matter interactions as well as applications of bio and chemical sensing.

Keywords: Field-directed self-assembly, core-shell nanoparticles, magnetic dipole-dipole interactions, mangetic-plasmonic and sensing application.

1 INTRODUCTION

The interest in the field-directed control of magnetic particles has grown steadily in recent years due to rapid advances in particle synthesis and related enabling technologies [1-2]. Applications in this field include gene transfection [3], drug delivery [4], and etc. Researchers have also explored the use of magnetic paticle self-assembly to enable chain-like structures for the scalable fabrication of nanostructured materials, e.g. for photonic [5], magnetic, optical and electronic applications [6]. Such an approach would open up opportunities for the low-cost high-throughput production of functional nanocomposite materials.

In this presentation we demonstrate a method for controlling the self-assembly of colloidal magnetic core-shell nanoparticles into chain-like structures with different constraints. We have demonstrated proof-of-concept of this method using a computational model that takes into account the dominant assembly mechanisms, including the induced magnetic dipole-dipole interactions, the electrostatic repulsion between particles due to the double layer forces based on DLVO theory, Brownian dynamics, Van der Waals interaction and a steric repulsive force caused by surfactant-surfactant contact. We found the electrostatic repulsion between particles due to double layer forces plays an imprtant role during the self-assembly process to form single chain structures instead of zip-chains. Furthermore, we performed an analysis of the localized surface plasmonic resonance (LSPR) in the chain of Fe_3O_4@Au nanoparticles. The results show a relatively uniform distribution of the thermal loss and highly localized electric field hot spots with an enhancement factor over 200 between adjacent nanoparticles. The ability to self-assemble the particles with tunable field enhancement holds potential for fundamental studies of light-matter interactions as well as applications of bio and chemical sensing, among others.

2 COMPUTATIONAL MODEL

Simulations were performed using the Monte Carlo method with the Metropolis algorithm to determine the final equilibrium particle structures of colloidal Fe_3O_4@Au particles after self-assembly. The approach was as follows. First, an initial configuration is generated consisting of randomly distributed particles. Each particle is then subjected to a random walk with a limited displacement step to generate a new position (x_{new},y_{new}, z_{new}) in the particle trail. The change in the total energy ΔU between new and initial configurations is then evaluated based on the particle displacement. The total energy U includes the magnetostatic U_m and magnetic dipole-dipole energies U_{dd}, electrostatic Energy U_e, Van der Waals potential energy U_v and a surfactant energy U_s that is computed when the particles are in contact. A uniform random number δ is

generated with $0<\delta<1$ and if $\delta<\exp(-\Delta U/k_B T)$, the particle displacement is accepted and the new particle configuration is adopted. This process is repeated until equilibrium is reached.

2.1 Magnetostatic Energy

The magnetostatic energy is predicted using an "effective" dipole moment method in which the particle is modeled as an "equivalent" point dipole with an effective moment $\boldsymbol{m}_{eff,i}$. The moment $\boldsymbol{m}_{eff,i} = V_{p,i} M_p$ is given by where $V_{p,i}$ and M_p is the volume and magnetization of the particle i, respectfully. For magnetic-dielectric core-shell particles, only the core contributes to that magnetic force and consequently, $\boldsymbol{m}_{eff,i} = V_{core,i} M_p$. The moment can be determined using a magnetization model that takes into account self-demagnetization and magnetic saturation of the particles[7]

$$\boldsymbol{m}_{i,eff} = V_{core,i} f(H_a) \boldsymbol{H}_a \tag{1}$$

where

$$f(H_a) = \begin{cases} \dfrac{3(\chi_p - \chi_f)}{(\chi_p + 2\chi_f)+3} & H_a < \left(\dfrac{(\chi_p + 2\chi_f)+3}{3(\chi_p - \chi_f)} \right) M_{sp} \\ M_{sp} / H_a & H_a \geq \left(\dfrac{(\chi_p + 2\chi_f)+3}{3(\chi_p - \chi_f)} \right) M_{sp} \end{cases} \tag{2}$$

In this expression, χ_f is the susceptibility of the fluid and χ_p is the intrinsic magnetic susceptibility of the particle, i.e. $M_p = \chi_p H_{in}$ where H_{in} is the field inside the particle. H_{in} differs from H_a by the demagnetization field i.e. $H_{in} = H_a - N_d M_p$ where N_d is the demagnetization factor of the particle, i.e. $N_d = 1/3$ for a spherical particle. The value of χ_p can be obtained from a measured M vs. H curve. However, M is often plotted as a function of H_a in which case $M_p = \chi_a H_a$, where χ_a is the apparent susceptibility. The two values of susceptibility are related as follows $\chi_p = \chi_a / (1 - N_d \chi_a)$, which reduces to $\chi_p = 3\chi_a / (3 - \chi_a)$ for a spherical particle.

Thus, a magnetic moment $\boldsymbol{m}_{eff,i}$ in an externally produced magnetic field $\boldsymbol{B}_a$ has a potential energy U_m,

$$U_{m,i} = -\boldsymbol{m}_{eff,i} \cdot \boldsymbol{B}_a \tag{3}$$

2.2 Magnetic dipole-dipole Interaction

A potential energy U_{dd} due to the magnetic dipole-dipole interaction can be discribed as the following equation,

$$U_{dd,ij} = -\frac{\mu_f}{4\pi} \left(3 \frac{(\boldsymbol{m}_{i,eff} \cdot \boldsymbol{r}_{ij})(\boldsymbol{m}_{j,eff} \cdot \boldsymbol{r}_{ij})}{r_{ij}^5} - \frac{\boldsymbol{m}_{i,eff} \cdot \boldsymbol{m}_{j,eff}}{r_{ij}^3} \right) \tag{4}$$

where $\boldsymbol{m}_{i,eff}$ and $\boldsymbol{m}_{j,eff}$ are the moments of i'th and j'th particle, respectively, and $\boldsymbol{r}_{ij}$ is the displacement vector between them. Note that $U_{dd,ij} \propto R_{core}^6$ for identical core shell particles. It is instructive to consider the nature of the dipole-dipole force ($\boldsymbol{F}_{dd,ij} = -\nabla U_{dd,ij}$) between identical paricles that have co-alligned moments that are induced by a uniform applied field as shown in **Fig. 1a**,**c**. One particle is located at the origin of a reference frame and we study the dipole-dipole force on a second particle as a function of its location in the x-y plane. **Figure 1c** shows the normalized dipole-dipole force field, i.e. a unit vector for the force on the second particle when it is located at any point in the x-y plane. Note that the dipole-dipole force can be attractrive or repulsive depending on the location of the particle, e.g. it is attractive when the particle is located at any point on y axis and repulsive when it is located on the x-axis. **Figure 1d** further illustrates the nature of the interparticle force (attractive or repulsive) with the particles at a fixed separation distance as a function of the angular coordinate θ of second particle, taken with respect to the y-axis.

2.3 Electrostatic Energy

The electrostatic repulsion between particles due to the double layer forces is described by the DLVO theory. A electrostatic energy is generated by[8],

$$U_{e,ij} = -2\pi\varepsilon\varepsilon_0 \left(\frac{k_B T}{ze} \right)^2 R_p q^2 \ln(1 - e^{-\kappa h_{ij}}) \tag{5}$$

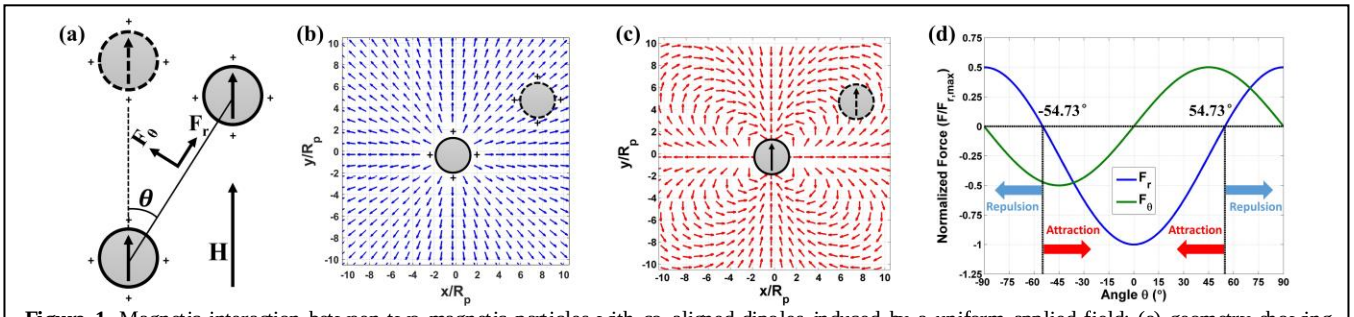

Figure 1. Magnetic interaction between two magnetic particles with co-aligned dipoles induced by a uniform applied field: (a) geometry showing relative position of interacting dipoles with surface charge and direction of applied field, (b) the electrostatic repulsion between particles due to the double layer forces (DLVO theory), (c) normalized (unit vector) dipole-dipole magnetic force field, (d) normalized dipole-dipole magnetic force components as a function of relative angular position θ as shown in (a).

Where ε is relative permittivity, ε_0 is the permittivity of free space, z is the valency of ions, e is the fundamental electronic charge, κ^{-1} is the Debye decay length given by $\kappa^{-1} = \sqrt{\frac{\varepsilon\varepsilon_0 k_B T}{2e^2 z^2 n_b}}$, n_b is the concentration of ions, q is the surface charge (which is scaled on $\varepsilon\varepsilon_0 k_B T\kappa / ez$). Note that, as shown in **Fig. 2b**, the electrostatic force ($\boldsymbol{F}_{e,ij} = -\nabla U_{e,ij}$) always acts as a repulsive force between two particles, which is important for different structures afer particles' self-assembly, i.e, zip-chains.

2.4 Van der Waals Potential Energy

Van der Waals potential Energy is calculated using[8],

$$U_{v,ij} = -\frac{A}{6}\left(\frac{2R_p^2}{r_{ij}^2 - 4R_p^2} + \frac{2R_p^2}{r_{ij}^2} + \ln\frac{r_{ij}^2 - 4R_p^2}{r_{ij}^2}\right) \quad (6)$$

where A is the Hamaker constant, R_p is the radius of the particle.

2.5 Surfactant Energy

A potential energy U_s is introduced into our our model due to the surfactant-surfactant contact, which is used to preclude particle overlapping during assembly,

$$U_s = 2\pi R_p^2 N_s k_B T\left\{2 - \frac{r_{ij} - 2R_p}{\delta} - \frac{r_{ij}}{\delta}\ln\left(\frac{2R_p + 2\delta}{r_{ij}}\right)\right\} \quad (7)$$

where R_p, δ and N_s are the radius of particle, the thickness of the surfactant layer and the surface density of surfactant molecules, respectively.

3 RESULTS

We use the monte carlo model to study the detailed 3D structures after self-assembly of core-shell particles. To demonstrate proof-of-concept we choose Fe_3O_4@Au core-shell particles, but note that the method broadly applies to multi-layered core-shell particles that have at least one magnetic component. The particle has a total radius of 25nm ($R_p = 25$ nm), with a 20 nm Fe3O4 core ($R_{core} = 20$ nm). Fe_3O_4 has a saturation magnetization $M_{sp} = 4.78\times10^5$ A/m and the applied external field is taken to be $H_a = 3.9\times10^5$ A/m ($B_a = 5000$ Gauss), which is sufficiently strong to saturate the nanoparticles as discussed below. To simplify the analysis, the carrier fluid is assumed to be nonmagnetic ($\chi_f = 0$). Periodic boundary conditions for particle transport are imposed at the lateral sides of the computation domain to enhance this model.

The magnetic particles form chain-like structures aligned with the applied uniform field in z direction as shown in **Fig. 2**, which is due to the minimum energy principle. From **Fig. 2a** and **b**, we find that the length of the particle chains can be concrolled by adjusting the height of nanochannel. When the height of the nanochannel changes from 300nm to 500nm, particles starts to self-assembly into a longer chain, i.e. 10 particles chain. Specifically, as the the volume fraction increases, more chains are forming as shown in **Fig. 2c** (φ = 1.96%) instead of 1.31% in **Fig. 2b**, which results in less speration spacing between chains. From the simulation results as shown in **Fig. 2d**, we see that the electrostatic repulsion between particles due to double layer forces plays an imprtant role during the self-assembly process. Zip-chain form with a reduced surface charge (1×10^{-18} C) instead of 5×10^{-18} C used in **Fig. 2a**, **b**, and **c**, as indicated by the red dashed circles.

A 3D computational photonic analysis is employed to investigate the optical properties in the 1D chain of Fe_3O_4@Au nanoparticles. In this section, we first explore the variation of the optical absorption cross section σ_{abs} in chains with different number of Fe_3O_4@Au nanoparticles. In **Fig. 3a**, we show that the LSPR wavelength of the chain strongly red-shifts as the number of chained nanoparticles increases. Interestingly, the peak resonant wavelength of a finite chain will asymptotically approach that of an infinite chain as the particle number increases. The stable optical response of a long chain necessarily qualify our 1D chain for a strong tolerance to the deviation of the channel height. On the other hand, microscopic studies of the light-matter interactions in the local region are necessary to reveal the compatibility of the 1D magnetic-plasmonic chain with

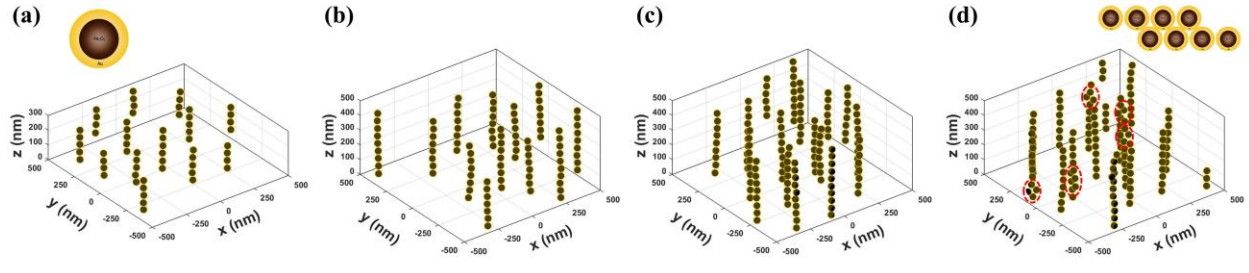

Figure 2. Magnetic particles' chaining with co-aligned dipoles induced by a uniform applied field: (a) at volume fraction of 1.31% in the nanochannel (confined to 300 nm), (b) at volume fraction of 1.31% in the nanochannel (confined to 500 nm), (c) at volume fraction of 1.96% in the nanochannel (confined to 500 nm), (d) at volume fraction of 1.96% in the nanochannel (confined to 500 nm), zip-chain is forming with a reduced surface charge, which is as cited by the red dashed circles.

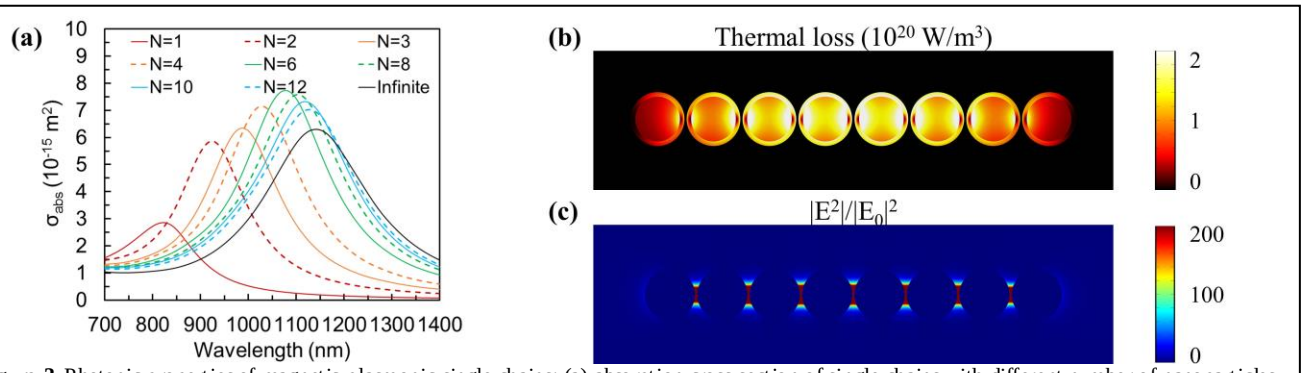

Figure 3. Photonic properties of magnetic-plasmonic single chains: (a) absorption cross section of single chains with different number of nanoparticles, (b) spatial profiles of thermal loss and (c) electric field enhancement in a single chain with eight mangetic-plasmonic nanoparticles.

important biomedical applications. **Fig. 3b** shows the spatial profile of the local thermal dissipation which is due to the absorption of the incident light. The local heating capability of the colloidal plasmonic nanoparticles have been harnessed in photothermal tranduction applications [9]. Our 1D magnetic-plasmonic chain possesses the obvious advantage over the randomly dispersed colloidal nanoparticles. For example, our chain not only dissipates the thermal energy efficiently in a specified spatial volume, it also exhibits a relatively uniform thermal dissipation profile along the chain. This advantage will provide a larger surface area for the attachment of thermal-responsive functional substances. In addition, LSPR-induced local field enhancement is an essential property in biosensing applications, since it can boost the efficiencies of Raman scattering, fluorescent labeling, and two-photon photoluminescence. **Fig. 3c**. is a plot of the local field enhancement profile. Since we consider an ultrathin functional polymeric layer outside each Fe_3O_4@Au nanoparticle, a nanogap exists between adjacent nanoparticles to concentrate the electric field strongly into a deep-subwavelength volume. The local field enhancement factor, i. e. $|E|^2/|E_0|^2$, can easily reach over a level of 200, therefore benefiting various biosensing applications.

4 CONCLUSIONS

We have described a method for directing the assembly of colloidal magnetic-dielectric core-shell nanoparticles into chain-like structures, which holds potential for biosensing applications due to various plasmonic effects. The electrostatic repulsion based on DLVO theory is a key feature of the method that enables forming single chain structures instead of zip-chains during the self-assembly process. A higher surface charge on the particles will provide more umiformly spaced-strucures after assembly, which is improtant for designing new functional materials. By controlling the predesigned nanochannel height, the length of the chain will be confined. The unique plasmonic responses of the 1D magnetic-plasmonic chain hold potentials for wide applications especially in photothermal transduction and biosensing.

ACKNOWLEDGEMENTS

The authors acknowledge financial support from the U.S. National Science Foundation, through award number CBET-1337860.

REFERENCES

[1] Pankhurst, Q.A.; Thanh, N.K.T.; Jones, S.K.; Dobson, J, "Progress in applications of magnetic nanoparticles in biomedicine." J. Phys. D Appl. Phys., 42, 224001, 2009.

[2] Berry, C.C, "Progress in functionalization of magnetic nanoparticles for applications in biomedicine." J. Phys. D Appl. Phys.,42, 224003, 2009.

[3] Furlani, E.P. and Xue, X, " Field, force and transport analysis for magnetic particle-based gene delivery." Microfluidics and nanofluidics, 13, 589, 2012.

[4] Arruebo, M; Fernández-Pacheco, R; Ibarra, M.R; Santamaría, J, "Magnetic nanoparticles for drug delivery." Nanotoday, 2, 22, 2007.

[5] Yethiraj, A.; Thijssen, J.H.J.; Wouterse, A.; Van Blaaderen, A, "Large-area electric-field-induced colloidal single crystals for photonic applications." Adv. Mater. (Weinheim, Ger.), 16, 596, 2004.

[6] Shipway, A.N.; Katz, E.; Willner, I, "Nanoparticle arrays on surfaces for electronic, optical, and sensor applications." ChemPhysChem, 1,18,2000.

[7] Xue, X.; Furlani, E.P, "Template-assisted nano-patterning of magnetic core–shell particles in gradient fields." PCCP, 16, 13306, 2014.

[8] Russel, W.B.; Saville, D.A.; Schowalter, W.R., "Colloidal Dispersions", Cambridge University Press, 1989.

[9] Kumar, C. S., & Mohammad, F, "Magnetic nanomaterials for hyperthermia-based therapy and controlled drug delivery." Advanced drug delivery reviews, 63, 789, 2011.